ADVANCED MATERIALS TECHNOLOGIES

Supporting Information

for *Adv. Mater. Technol.*, DOI: 10.1002/admt.202000431

Electrohydrodynamic Jet Printing of 1D Photonic Crystals: Part II—Optical Design and Reflectance Characteristics

*Brian Iezzi, Zahra Afkhami, Shea Sanvordenker, David Hoelzle, Kira Barton, and Max Shtein**

Supporting Information

Electrohydrodynamic Jet Printing of One-Dimensional Photonic Crystals: Part II – Optical Design and Reflectance Characteristics

Brian Iezzi, Zahra Afkhami, Shea Sanvordenker, David Hoelzle, Kira Barton, Max Shtein[*]

Table S1: Comparison of polymeric and sol-gel based materials for potential 1DPCs

High Index Material, n_H	Low Index Material, n_L	Optimal Thickness t_H/t_L (nm) for 1DPC at 550 nm	Approx. Refractive Index Contrast (Δn) at 589 nm	Curing Method
Polystyrene (PS),1.56	Polyvinyl Pyrollidone (PVP), 1.50	88/92	0.06	Thermal Anneal at 110°C [32]
Polyvinyl Carbazole (PVK), 1.66	Cellulose Acetate (CA), 1.48	83/93	0.18	Thermal Anneal at 80°C [9]
Titania (TiO_2) Sol-Gel, 2.34	Silica (SiO_2) Sol-Gel, 1.48	57/93	0.86	Thermal Anneal at 400°C [28]
NOA170, 1.70	NOA1348, 1.35	81/102	0.35	UV Light cure at 365 nm [33]
NOA170, 1.70	Loctite 3526, 1.51	81/91	0.19	UV Light cure at 365 nm [33]

Table S2: Optical Peak Shifts for Spatial OM Analysis in Figure 4

E-jet Printed Layer 1: NOA170 Layer 2: Loctite	Peak Reflectance (%)	Peak Reflectance (nm)
B1	37.5±1.6	439.0±7.0
B2	31.5±1.6	429.9±4.8
G1	32.9±4.2	515.2±18.2
G2	26.3±1.8	494.3±15.4
R1	23.5±3.5	673.1±5.0
R2	25.1±3.2	670.6±5.3

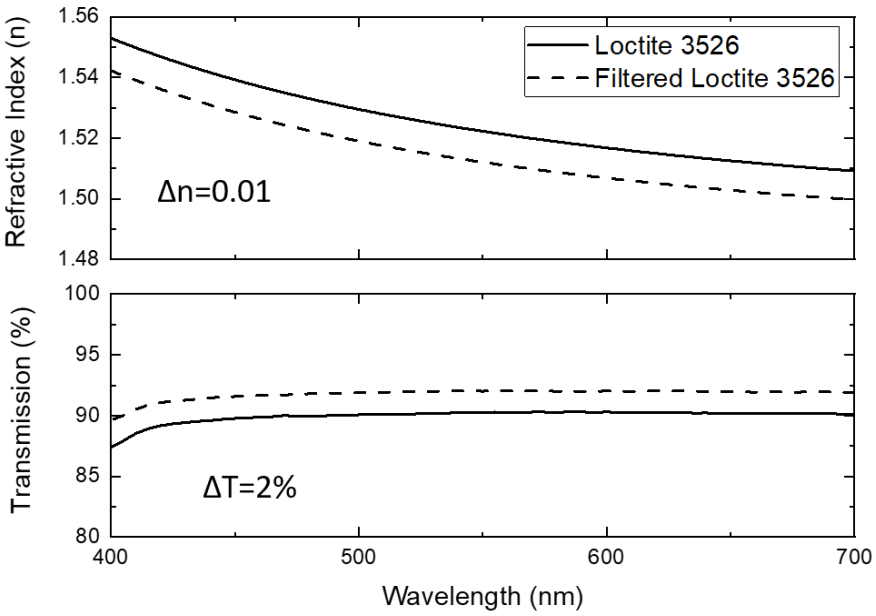

Figure S1: Refractive index (top) and transmission (bottom) change after filtering Loctite 3526. There is a slight decrease in refractive index as well as an increase in transmission. This is believed to be due to the removal of some longer molecular chain resin from the Loctite formulation which should increase transparency and decrease refractive index.

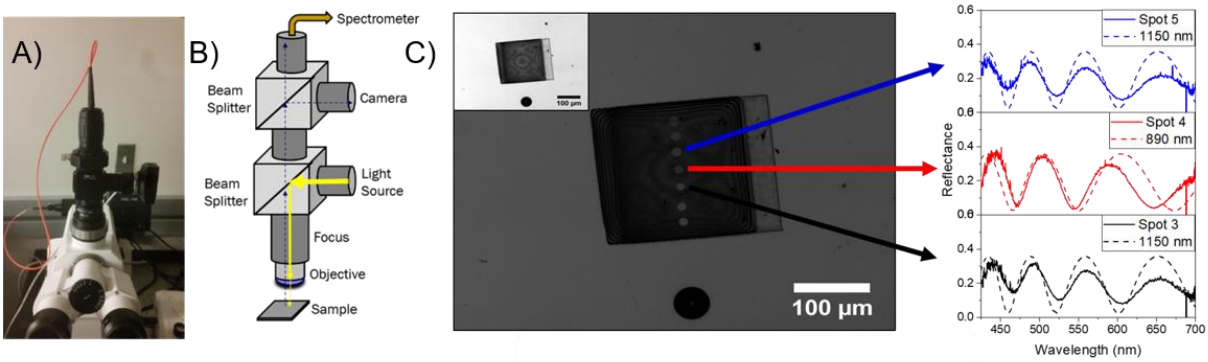

Figure S2: A) Optical microspectroscopy (OM) setup mounted on the trinocular of a Zeiss AxioScope optical microscope B) Breakdown of OM setup. Light (solid yellow arrows) first passes from a halogen light source to a 50/50 beam splitter. The split beam then is focused by a 10x or 50x objective onto the sample surface and then used to collect the reflected light (dashed blue arrow). This light passes back through the first beam splitter (with loss) and then on to a 90/10 beamsplitter. 10% of the signal is sent to a CMOS camera for sample focusing/acquisition while 90% is sent to a spectrometer via a 50 µm optical fiber for processing. C) Optical micrograph showing sampling locations via OM setup (original image inset). Plots demonstrate that the system can be used for assessing topological information of a printed sample.

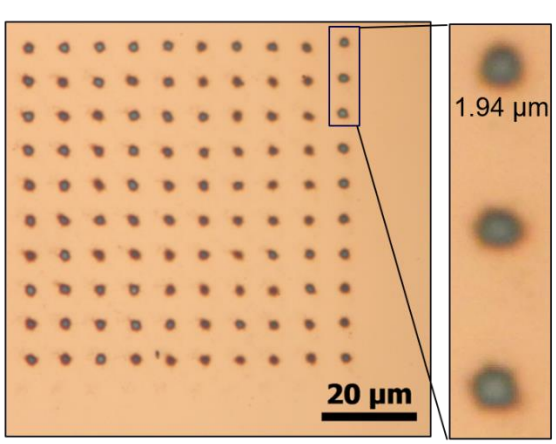

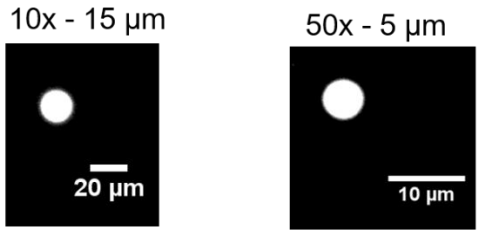

AFM Image	Sampling Area Diameter (µm)	AFM Measured Thickness (nm)	σ_{RMS} (nm)
1	29	158.6	11.4
2	9.7	155.3	8.1
3	2.4	155.9	6.6

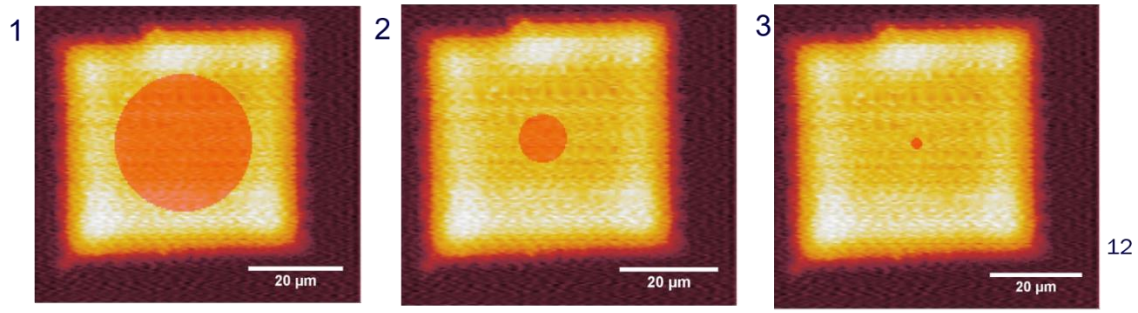

Figure S3: Comparison of printed droplet diameter to sampling area of optical microspectroscopy (OM) setup. Sampling diameter for the 10x objective was around 15 micrometers (upper center micrograph). Droplets are around 2 micrometers in diameter. AFM images with masks corresponding to the size of the OM sampling area are used to determine the variation in RMS surface roughness depending on area. There was minimal change with roughness decreasing from 11.4 nm to 6.6 nm from 29 micrometer diameter to 2.4 micrometer diameter. Optical simulations have shown this small amount of surface roughness has minimal affect on reflectance response.

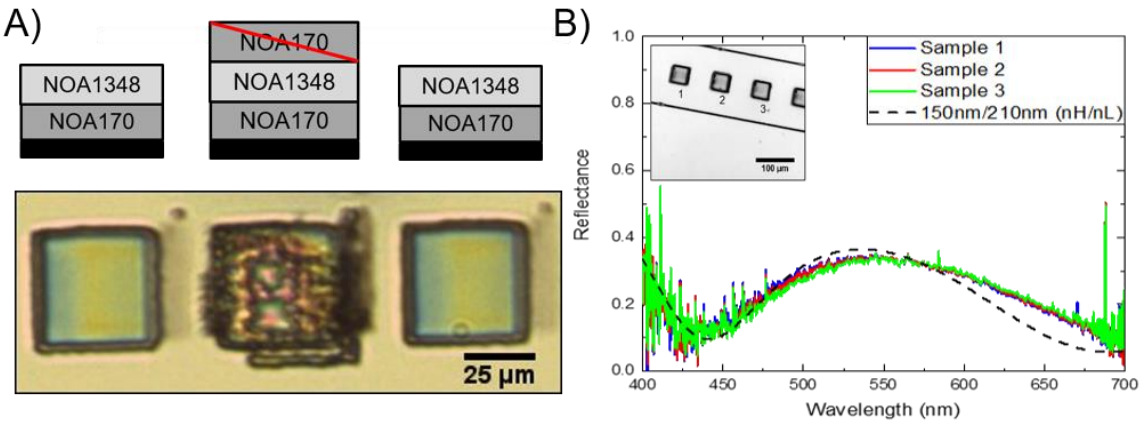

Figure S4: A) Attempt at merging NOA170 on top of a previously printed NOA1348 layer showing poor merging behavior. B) Inset - Optical micrograph of three dual layer NOA170/1348 samples with reflectance sampling points indicated by number and Graph: Reflectance response of three samples across the visible spectrum showing uniformity along with transfer matrix simulations matching the AFM data collected for the same sample

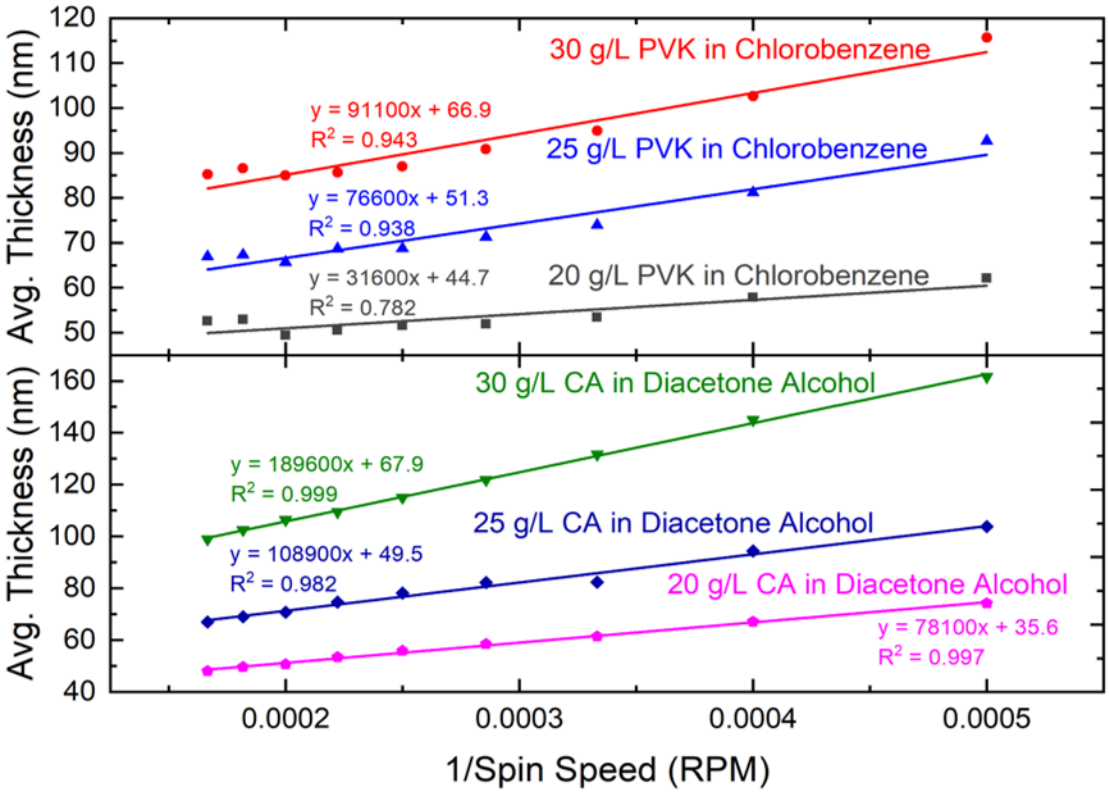

Figure S5: Empirical model for manufacturing spin-coated PVK/CA dual layer samples. Relatively thick (>150nm) layers of CA require high concentrations and low spin speeds thus leading to a higher likelihood of inaccuracies in the model as evidenced in the blue spin-coated samples.

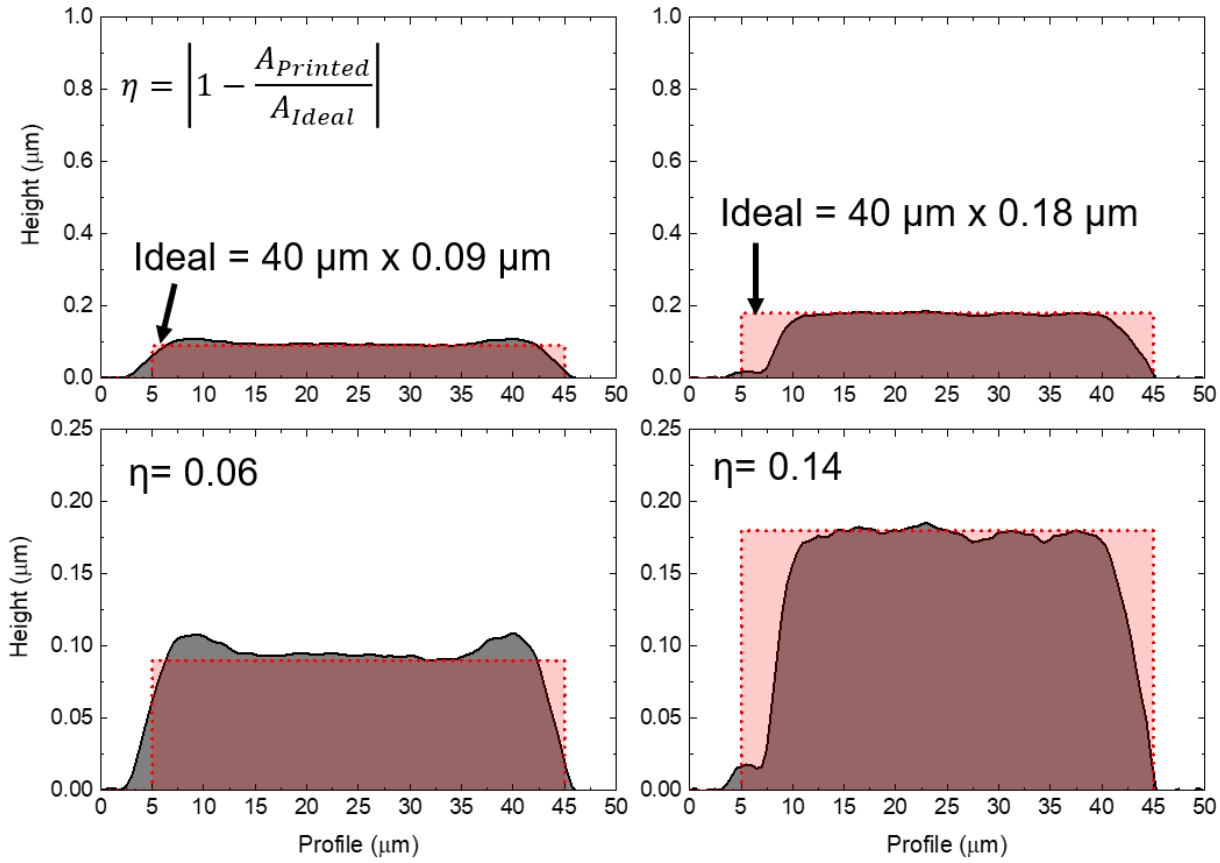

Figure S6: Investigation of edge sharpness in printed pixels. The printed first and second layer for a typical "blue" sample (NOA170/Loctite) with the AFM-measured cross section and the ideal rectangular cross section. The deposit shape factor, η, is defined as the ratio of the printed cross sectional area to the ideal cross sectional area. The top figures show the low aspect ratio of these deposits while the bottom figures show the deposit shape factor is farther from 1 (a perfect deposit) for the second layer than the first.

Pixel Size (Area)	Number of Samples (N)	Average Measured Area (μm^2)	Standard Deviation of Measure Area (μm^2)	Percent Error from Ideal Pixel Area (%)
40 µm x 40 µm (1600 μm^2)	16	1587.7	81.6	0.77
13 µm x 13 µm (169 μm^2)	12	161.6	3.4	4.4

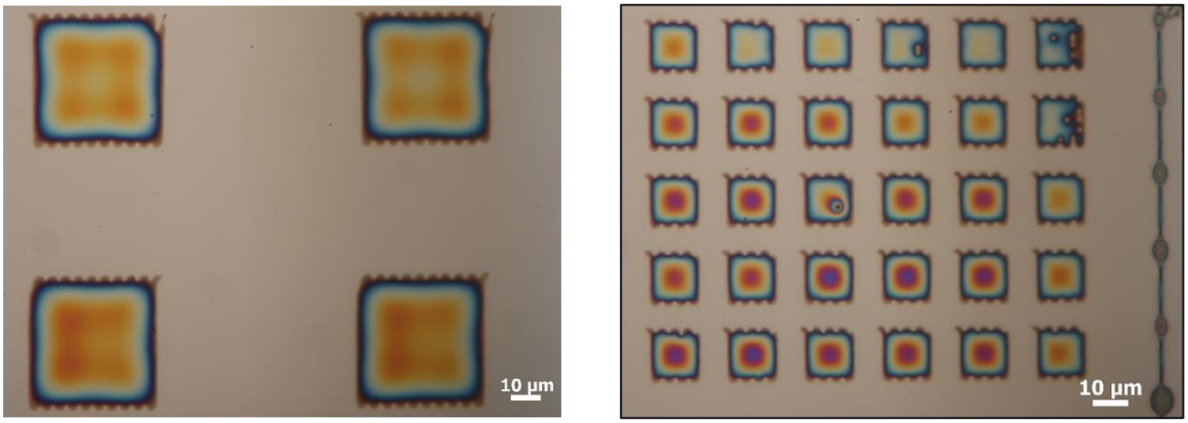

Figure S7: Analysis of Spatial Error Pixels with varying sizes of 40 micrometers by 40 micrometers (example bottom left) and 13 micrometers by 13 micrometers (example bottom right)

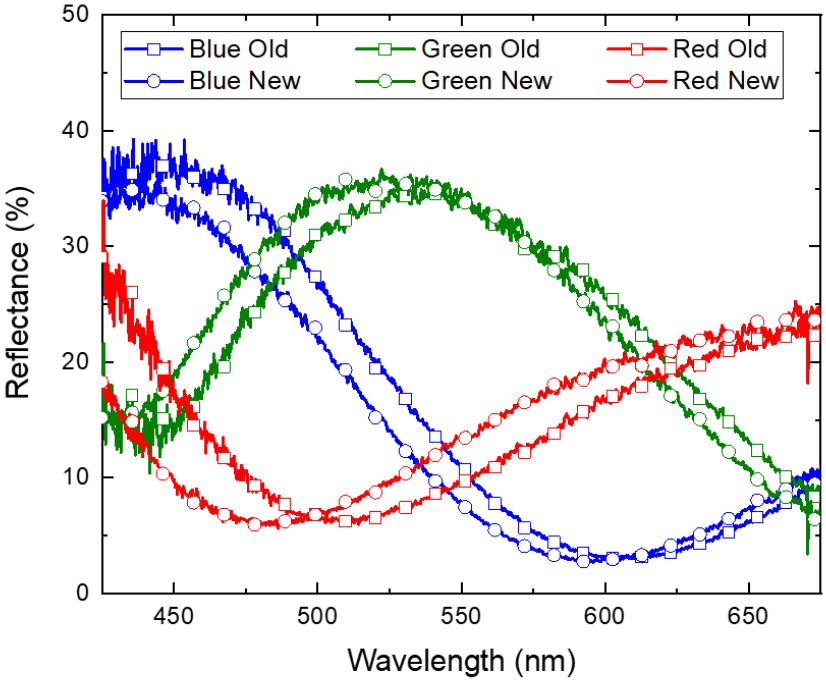

Figure S8: Comparison of printed bi-layer samples after 1 year in ambient conditions. Minor shifts in reflectance spectra occurred for all three samples. Possible reasons for shifts include changing of the lamp light source over the course of the year.